

Nanoscale

Accepted Manuscript



This is an *Accepted Manuscript*, which has been through the Royal Society of Chemistry peer review process and has been accepted for publication.

Accepted Manuscripts are published online shortly after acceptance, before technical editing, formatting and proof reading. Using this free service, authors can make their results available to the community, in citable form, before we publish the edited article. We will replace this *Accepted Manuscript* with the edited and formatted *Advance Article* as soon as it is available.

You can find more information about *Accepted Manuscripts* in the [Information for Authors](#).

Please note that technical editing may introduce minor changes to the text and/or graphics, which may alter content. The journal's standard [Terms & Conditions](#) and the [Ethical guidelines](#) still apply. In no event shall the Royal Society of Chemistry be held responsible for any errors or omissions in this *Accepted Manuscript* or any consequences arising from the use of any information it contains.



Nanoscale

ARTICLE

Extremely Low-Index Photonic Crystal Layer for Enhanced Light Extraction from Organic Light-Emitting Diodes

Yong Sub Shim,^a Ju Hyun Hwang,^a Kyu Nyun Kim,^a Cheol Hwee Park,^a Sun-Gyu Jung,^a Bong Han Bae,^a Dong Jun Lee,^a Chan Hyuk Park,^a Young Wook Park^{b*} and Byeong-Kwon Ju^{a*}

Received 00th January 20xx,
Accepted 00th January 20xx

DOI: 10.1039/x0xx00000x

www.rsc.org/

This paper reports organic light-emitting diodes (OLEDs) with improved light extraction fabricated by embedding an extremely low-index photonic crystal (LIPC) layer. The LIPC layer increases the optical efficiency through the reduced wave-guide mode between substrate and anode both by increased light resonance and by strengthened diffraction effect from an extremely low-refractive-index medium, specifically a line structure composed of vacuum gap. As a result, the current efficiency and power efficiency of the LIPC-OLEDs are 1.51 and 1.93 times higher, respectively, than the reference device at 1000 cd/m². Because most of the light extraction is significant, especially in forward direction, at the specific wavelengths satisfying Bragg's diffraction equation, it is possible to calculate the anomalous spectrum of the LIPC-OLED through the finite-difference time domain (FDTD) method.

Introduction

Organic light-emitting diodes (OLEDs) have been spotlighted as a next-generation display technology because of their self-emitting characteristics, excellent color gamut, high-speed operation, and applicability to flexible or stretchable devices. According to these recent trends, numerous efforts for improving the functionality of the OLEDs are being actively implemented to increase the commercial potential and extend the application range to not only mobile and large flat-panel displays, but also to environmentally friendly general lighting and automotive lighting. However, limitations in the optical efficiency and manufacturing yield have impeded the spread of this new technology, and so far it is narrowly used in high-end products with high cost.¹⁻³

Generally, the optical efficiency of OLEDs can be evaluated by the value of external quantum efficiency (η_{EQE}), which is calculated as the product of internal quantum efficiency (η_{IQE}) and light out-coupling rate (η_{coupling}):⁴

$$\eta_{\text{EQE}} = \eta_{\text{IQE}} \times \eta_{\text{coupling}} \quad (1)$$

In the first generation OLEDs, made of fluorescent materials, the η_{IQE} was up to 25% because only the singlet states of excitons can be emitted in the form of light. However, the development of phosphorescent OLED materials as the second generation enabled it

theoretically to reach 100% by utilizing both singlet and triplet states of excitons through the intersystem crossing (ISC) process.⁵ Recently, with the appearance of thermally activated delayed fluorescent materials, which are the so-called third generation OLEDs, it is also possible to dramatically increase the efficiency of fluorescent emission by promoting the condition of reverse-ISC.⁶ In conclusion, the rate of η_{IQE} already converges to 1 in theory, as identified in previous studies in the chemistry and materials science fields.

Therefore, the importance of η_{coupling} as a degree of how many generated photons can be extracted out of the device without loss has been emphasized. Because of multi-stacked thin films with different refractive indices (RIs), about 80% of generated photons are lost while passing through each OLED film as wave-guided modes affected by the total internal reflection. In order to minimize such losses, various advanced structures have been developed as internal or external light extraction layers, such as the random patterned structure, periodic photonic crystal (PC) structure, micro-lens array, and low-index grid, to improve the coupling rate.⁷⁻¹¹

Here, we researched the extremely low-index photonic crystal layer (LIPC), specifically regarding more efficient ways to utilize its periodic structure in accordance with the refractive index difference (n_{diff}) between two media constituting the PC. Because the extremely LIPC layer, consisting of a vacuum gap with an RI of 1.0, is situated between the indium tin oxide (ITO) and a glass substrate with high RIs (approximately 1.9 and 1.5, respectively), the n_{diff} can theoretically have a maximum value. This structure can be simply built by laser interference lithography (LIL), which enables low-cost manufacturing for a maskless and largely scalable process. By inserting this ultra-low RI structure, the optical efficiency of the OLED device is significantly enhanced without any roll-off phenomenon and can be analyzed by both the aspects of RI matching

^a Display and Nanosystem Laboratory, College of Engineering, Korea University, Seoul 136-713, Republic of Korea, E-mail: bkju@korea.ac.kr; Fax: +82-3290-3671; Tel: +82-3290-3237

^b The Institute of High Technology Materials and Devices, Korea University, Seoul 136-713, Republic of Korea, E-mail: zerook@korea.ac.kr; Fax: +82-3290-3665; Tel: +82-3290-3665

*Electronic Supplementary Information (ESI) available: See DOI: 10.1039/x0xx00000x

in geometric optics and tremendous PC diffraction in nanoscale optics. The changes in the spectrum are inevitable because Bragg's diffraction and strengthened resonance effect is highly significant, but the peaked wavelength point is approximately predictable with the help of finite-difference time domain (FDTD) numerical calculation. Conversely, if designed for an application such as quantum dot or multi-color OLEDs requiring specific wavelength enhancement, this novel structure will be applicable as a more powerful approach.

Experimental

Schematic diagrams of the entire manufacturing process are shown in Figure 1. First, we made a periodic nanopatterned structure on the photoresist (PR; AR-N 4240, Allresist Co., Ltd) with a thinner (AR 300-12, Allresist, Co., Ltd) spin-coated Eagle XG glass via laser interference lithography using a Lloyd's mirror. Because a frequency-doubled Ar-ion laser ($\lambda_{Ar} = 257$ nm; fixed) was used as the exposure light source, the period of the nanopattern (Λ ; pitch) is determined only by the exposure angle (θ) between the laser beam and the plane of the mirror.¹²

$$\Lambda (\text{pitch}) = \frac{\lambda_{Ar}}{2 \sin \theta} \quad (2)$$

The height of the PR, which becomes the depth of the LIPC layer, depends on the diluted ratio of the PR solution consisting of the PR and the thinner, which is used as a solvent. It is well known that a deeper PC layer causes more light extraction.^{13, 14} However, in order to maintain the electrical stability of the OLEDs,^{15, 16} the depth was fixed at 100–110 nm by mixing the PR and thinner in a ratio of 1:4 (refer to supporting information).

Above the nanopatterned PR, 300-nm-thick ITO was deposited by a radio-frequency sputtering process with high step coverage. Then, to make the vacuum gap between the ITO and glass, the PR was completely eliminated in the conditions of an ultrasonic bath filled with a PR-remover and acetone mixture for 10 min. Additional vacuum heat treatment at 300 °C for 30 min and O₂ plasma

treatment is essential to help the recrystallization of ITO film and to remove the PR residue.¹⁷

After thermal evaporation in high vacuum (10^{-6} Torr) for depositing organic materials (60-nm-thick N, N'-Bis (naphthalen-1-yl)-N, N'-bis (phenyl)-benzidine (NPB) as an HTL, 80-nm-thick tris (8-hydroxy-quinolino) aluminum (Alq₃) both as ETL and EML) and the layers constituting the cathode (0.5-nm-thick LiF and 100-nm-thick Al), the green emissive OLEDs with LIPC were successfully produced.

Figure 2 shows scanning electron microscope (SEM) images and a photograph of the main manufacturing steps. Figure 2(a) is an image corresponding to step P-5 in Figure 1. Before the PR removal process, it can be seen that corrugated ITO film was deposited on the nanopatterned PR having a period of 720 nm (LIL exposure angle, $\theta \sim 10^\circ$).

As shown in Figure 2(b) and 2(c) corresponding to the step P-6 in Figure 1, the vacuum gap forming the LIPC is perfectly created between the substrate and ITO interface. It should be noted that there remains a clear spectrum distortion like a prism because the pitch of the nanopattern is in the visible wavelength range and the RI difference ($n_{diff} \sim 0.9$) between the media constituting the PC layer is exceedingly large.¹⁸⁻²⁰

Because the step coverage of the sputtering process is too high, the crystal growth of the ITO film is significantly affected by the PR shape. When the PR is formed into the undercut profile, the sheet resistance of the corrugated ITO can be unintentionally raised 10 times higher than flat ITO. Therefore, the nanopattern of the PR formed by LIL must be a tapered (or rounded) shape rather than an undercut profile adjusted by increasing the energy of the laser to more than 35 mJ/cm² and by adding heat treatment at 150 °C for reflow of the PR (refer to supporting information). Also, 300-nm-thick ITO, which is much thicker than conventional OLEDs, helps maintain the durability and uniformity of the electrode by forming some degree of planarization.

When these conditions are met, the electrical characteristics of the corrugated anode were improved depending on the increase in electric field, which results in enhanced operating voltage and

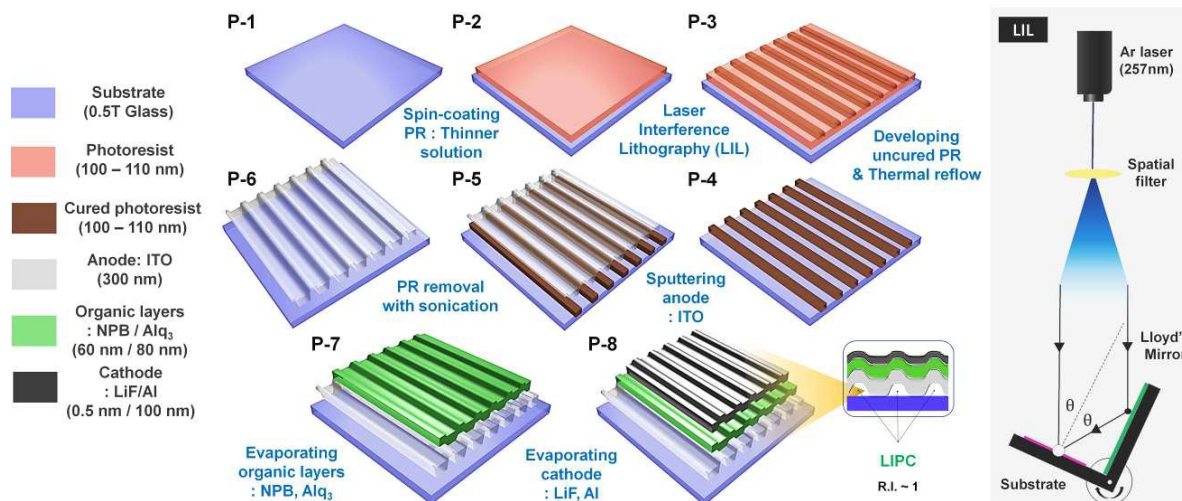


Figure 1. Schematic diagrams of the fabrication of LIPC-OLEDs and the principle of the LIL system using a Lloyd's mirror interferometer.

current density of the LIPC-OLED.¹⁶

Finally, it was confirmed that each layer of the OLED was well stacked along the corrugated pattern as shown in Figure 2(d)

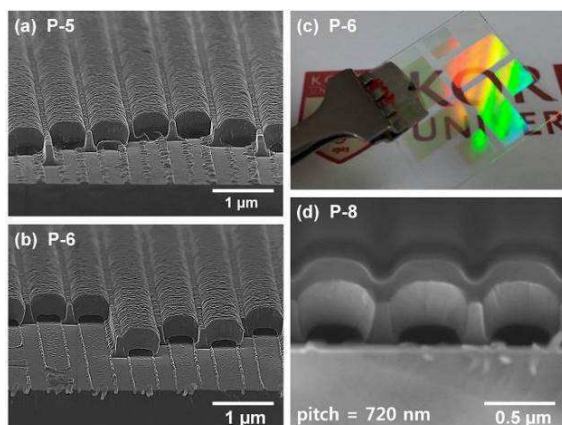


Figure 2. SEM images and photograph in the manufacturing process, corresponding to (a) P-5 (before PR removal); (b), (c) P-6 (after PR removal); and (d) P-8 (the cross-section view of LIPC-OLED) in Figure 1, respectively. The LIPC pitch is 720 nm

Results and discussion

Optical effects of LIPC

In this study, the main element of the light extraction is the high RI difference (n_{diff}) of the media forming the PC layer. Because the ITO film and vacuum gap have RIs of 1.9 and 1.0 on average in the visible wavelength, the extremely LIPC layer has the maximum RI difference ($n_{\text{diff}} = 0.9$) that is possible in the PC structure.

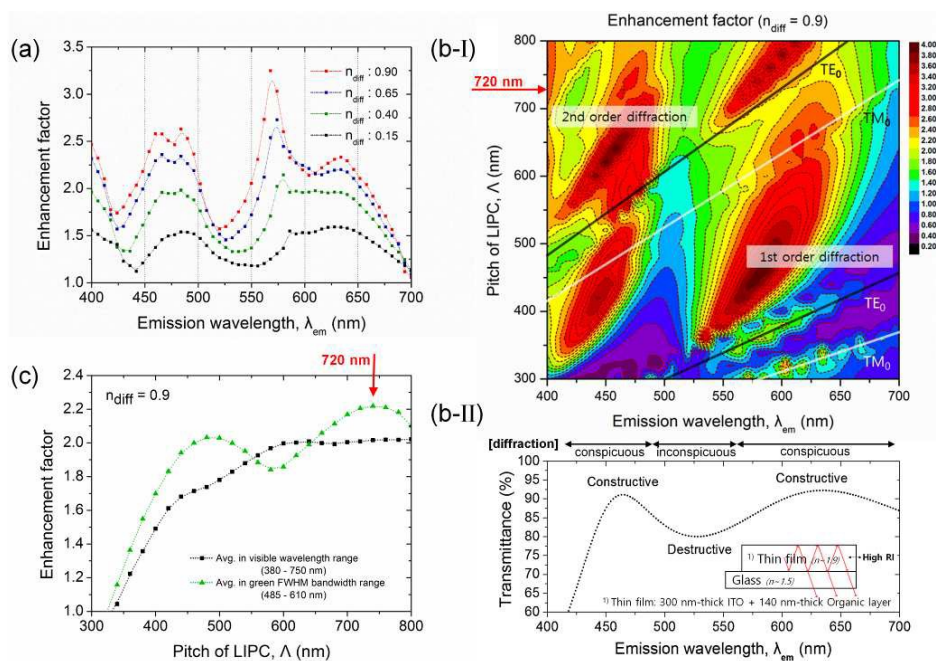


Figure 3. Results of FDTD simulation: (a) Enhancement factor-emission wavelength graph per RI difference when the LIPC pitch is fixed at 720 nm, (b-I) contour plot of enhancement factor as a function of pitch (Λ) and emission wavelength (λ_{em}), and (b-II) the internal resonance effect of high index thin film which explains the partially concentrated Bragg's diffraction in LIPC-OLED. (c) Average enhancement factor on the whole visible range and on the green FWHM bandwidth range due to changes in pitch. All the values are calculated relative to the straight direction of photons inside the air-light cone of 15°.

In order to visualize the optical effects of such a low index layer, a two dimensional FDTD simulation which is suitable for nano stripe periodic pattern was used. Structurally, the width ratio of vacuum gap was defined as 60% of the total light-emitting area in all pitch conditions. The enhancement (of light extraction) factor of each structure was calculated as the ratio of the integrated electric field intensity (E^2) by fixed far-field monitor. To implement the properties of the sheet light source of actual OLED, each randomly distributed (x-coordinate) and oriented (x-, y-, and z-polarized) dipole was case by case simulated, and the mean value was taken.¹²

Figure 3(a) shows the simulation results of the enhancement factor as a function of the emission wavelength when the pitch of the LIPC is 720 nm. The peaked emission wavelength of the PC structured OLED in the straight direction (low viewing angle) is mostly determined by the pitch rather than by the n_{diff} considering the degree of change of each parameter according to the abbreviated Bragg's equation:^{21, 22}

$$\Lambda(\text{pitch}) = \frac{\lambda_{\text{em}}}{n_{\text{eff}}} \cdot m, \quad n_{\text{eff}} \propto \frac{1}{n_{\text{diff}}} \quad (3)$$

where the n_{eff} is the effective refractive index of PC media, λ_{em} is the emission wavelength, and m is an integer value. Thus, there is little difference in peaked emission wavelength by n_{diff} . Only a small red shift is found because the high n_{diff} indicates that the n_{eff} is contrarily low by using extremely low RI media.

On the other hand, the intensity shows a large difference by n_{diff} . The higher n_{diff} shows a higher enhancement factor, whereas the sharp-waved curve caused by the high peak-to-peak value is thought to make an inevitable spectral reinforcement at the specific wavelength when applied to the OLEDs. In contrast, the low n_{diff} shows an even improvement in the whole visible wavelength range, but the ratio is relatively low. These indicate that using extremely LIPC can maximize the optical efficiency in terms of numerical concepts; after a comprehensive judgment, we focused more on the light extraction characteristics of LIPC-OLEDs, including the information about various pitches and angular distribution, despite disregarding some amount of unavoidable spectrum distortion.

Figure 3(b-I) shows a contour plot of enhancement factor due to changes in LIPC pitch and emission wavelength with the auxiliary lines reflecting Bragg's diffraction equation. Depending on the transfer matrix method analysis,²³ one transverse magnetic (TM_0) mode and one transverse electric (TE_0) mode of the field are the most influential components leading to wave-guiding in flat OLEDs. However, when the PC grating is applied, the TM_0 mode, generally maximized at the organic and cathode interface, can be largely extracted by the out-coupled surface plasmon polaritons. The n_{eff} in this part, which is mostly composed of organic material, is high (approximately 1.9), and the TM_0 line satisfying Equation 3 has a relatively low gradient. On the other hand, the intensity of the TE_0 mode is maximized near the ITO layer, attributed to the high RI. The n_{eff} near the ITO is approximately 1.8 in general OLEDs, but is reduced to 1.5–1.6 by inserting the extremely LIPC layer. For this reason, the TE_0 line of the LIPC-OLED has a higher gradient than that of the general case. If the pitch is shorter than 400 nm, the improvement is dominated by the first-order diffraction, and by the second-order diffraction for the opposite case.

Even if the backgrounded contour plot of Figure 3(b-I) is the comprehensive result reflecting a variety of complex optical effects as well as Bragg's diffraction, it was found that the tendency of the first-order diffraction exactly matches the PC

theory. However, the tendency of the second-order diffraction follows the trend only limited to the specific wavelengths, so it breaks the perfect linear relationship between the emission wavelength and pitch of PC. There is an additional prominent factor to be considered in the area of higher pitch. As described in Figure 3(b-II), the optical transmittance of thin film has some fluctuation according to the wavelength because of the light resonance inside high RI film, surrounded by low RI films. In this perspective, the inserted LIPC will provide more significant increase in the resonant amplitude because it makes the most part of ITO directly contact with the vacuum gap instead of glass substrate. Consequently, concentrated PC diffraction with higher slope than expected is observed in the region where the internal resonance is constructive, while it is relatively inconspicuous in the region of destructive condition.

Based on the information of Figure 3(b), we obtained the average enhancement factor in the visible wavelength range and in green FWHM bandwidth range as shown in Figure 3(d) according to the extremely LIPC pitch in the range of 300 nm–800 nm, where the PC diffraction is dominantly represented. Although there is some fluctuations when narrowing to a more specific colour wavelength range, it can be obviously seen that the enhancement starts to sharply decline below a pitch of 400 nm where the serious resonance effect do not appear anymore. Consequently, we concluded using a higher pitch (720 nm; in this experiment for green OLED) is the best way to increase the optical efficiency of the LIPC-OLED consistent with the initial design.

As detailed in Figure 4(a) and 4(b), which are angular distributions simulated by p-polarized and s-polarized dipoles, respectively, the intensity increase of the TM_0 mode stands out at an emission wavelength of 570 nm and that of the TE_0 mode stands out at 485 nm. This means that the two protruded peaks at the blue and orange-red wavelength range came from each mode affected by Bragg's diffraction which is more reinforced by satisfying internal resonance condition of high RI film. That is, the LIPC is quite an adequate structure able to extract both major modes with respect to the light with straight direction.

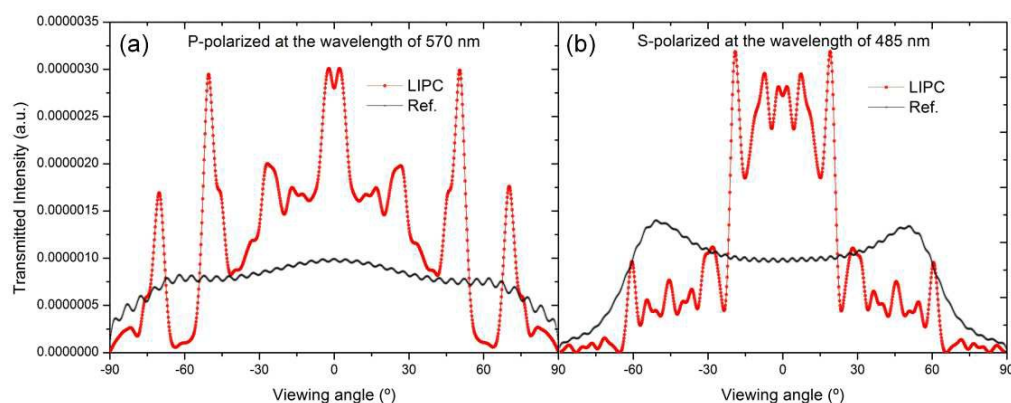


Figure 4. Angular distribution of each mode at specific wavelengths corresponding to Bragg's equation. The condition of pitch is fixed at 720 nm, which exhibits the highest extraction efficiency. (a) P-polarized dipoles (for TM_0 mode) at the wavelength of 570 nm (orange-red), and (b) s-polarized dipoles (for TE_0 mode) at the wavelength of 485 nm (blue) were simulated. The improvement of the p-polarized dipoles is present in the wide range of viewing angle affected by the diffraction, whereas that of the s-polarized dipoles is intensively distributed in the low viewing angle.

Electroluminescence Characteristics

The electroluminescence (EL) characteristics of OLED devices according to the presence of the LIPC are presented in Figure 5 and summarized in Table 1. They were measured by a PR-670 (SpectraScan, Photo Research, Inc.) spectroradiometer in a dark box with an adjustable voltage source (Model 237, Keithley Instruments, Inc.). Due to the limited measurement conditions, most of the presented values were measured in the perpendicular direction except the angular distribution measured at the discrete angles of 10°, 20°, 30°, 40°, 50°, 60°.

On the basis of the simulation results, an LIPC-OLED with a period of 720 nm, and a conventional flat OLED without PC structure (as reference), were fabricated as in the insets in Figure 5(c). Each layer's thickness of the two devices is the same in the equivalent deposition conditions. The current density of the LIPC-OLED is much higher at the same voltage because of a stronger electric field caused by a partially reduced current path resulting from the sinusoidal corrugated pattern of the electrode. Even though the corrugation affects quite a few unstable current uniformity at low voltage, the LIPC-OLED exhibits a noticeable increase compared with the reference device in current efficiency (51.3% increase), power efficiency (92.6% increase), and external quantum efficiency (34.0% increase) at the light-emitting step (at 1000 cd/m²).

The reasons for the high optical efficiency can be analyzed in two ways. First, the influence of PC diffraction, which is prominently identified in the spectral graph of EL intensity, is dominant. Through the previous simulation section, it was possible to estimate the spectrum of the LIPC-OLED as

$$\alpha \times \text{Enh}(n_{\text{diff}}, \lambda_{\text{em}}) \times I_{\text{ref}}(\lambda_{\text{em}}) = I_{\text{LIPC}}(\lambda_{\text{em}}) \quad (4)$$

where α is the calibration coefficient, and Enh is an abbreviation for “enhancement factor,” whose data was obtained from Figure 3(a). I_{ref} is the normalized EL intensity of the reference device, and I_{LIPC} is the estimated EL intensity of the LIPC-OLED as a function of emission wavelength. Figure 6 shows the comparison between the calculated spectrum in this method and the actual spectrum of the fabricated LIPC-OLED and both results were almost identical when compensated by the calibration coefficient ($\alpha = 0.654$). Because the increase in intensity is higher at larger n_{diff} , there are much sharper spectral peaks that are difficult to offset. Actual wavelength peaks were found near the blue (490 nm) and orange-red (574 nm) range, similar to the simulation reflecting the Bragg's equation (the enhancement factor outside the FWHM wavelength range of the green OLED is almost negligible), and namely, this comparison of numerical results proves that the main point of the sharp optical enhancement at the specific wavelength is contributed from the PC diffraction.

Next, the inserted extremely low RI layer changes the path of the light in the vertical direction geometrically since the widely existed vacuum gaps (RI = 1) provide further enhanced light resonant condition by the drastic RI difference between adjacent films. Due to this resonance, the diffraction is stronger in place satisfying the constructive condition, and it contributes to the broader bandwidth of spectral peak than affected only by the Bragg's diffraction. Moreover, each line of the LIPC that is densely arranged in nano-size makes most of the emitted light encounter the vacuum gaps. These concepts of RI matching can extract the substrate waveguide mode by reducing the light incidence angle less than the critical angle.^{11,24} They were also observed in that the intensity of s-polarized dipoles in the low viewing angle is very high, whereas the intensity in a high viewing angle is lower than the reference, as in Figure 4(b).

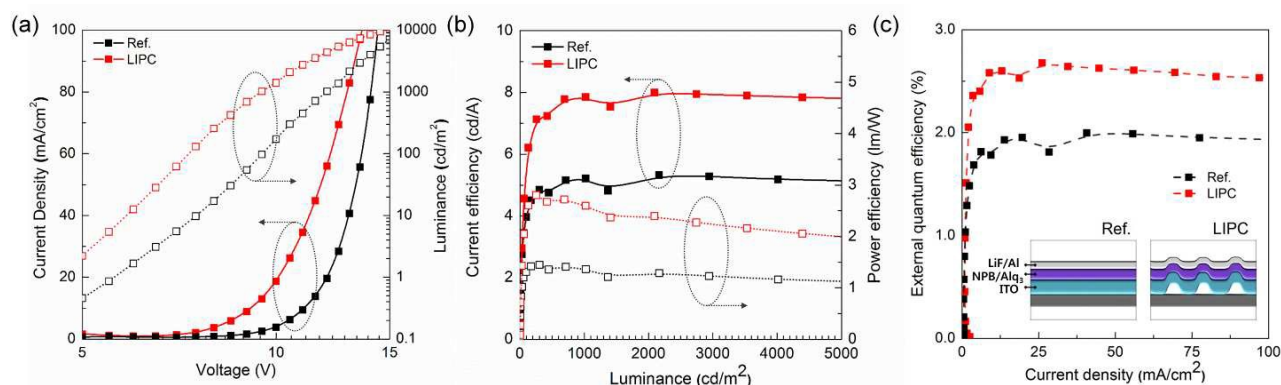


Figure 5. EL characteristic of the reference (black line) and LIPC-OLED (red line) whose schematic diagrams are shown in the insets of (c). Each plot shows (a) I-V and V-L characteristics, (b) current and power efficiency as a function of luminance, and (c) external quantum efficiency as a function of current density.

Table 1. Summary of EL characteristics of fabricated OLEDs.

	Current efficiency (cd/A)		Power efficiency (lm/W)		External quantum efficiency (%)	
	at 1,000 cd/m ²	at 5,000 cd/m ²	at 1,000 cd/m ²	at 5,000 cd/m ²	at 1,000 cd/m ²	at 5,000 cd/m ²
Ref.	5.19	5.14	1.36	1.13	1.94	1.93
LIPC	7.85 (51.3% ↑)	7.82 (52.1% ↑)	2.62 (92.6% ↑)	2.01 (77.9% ↑)	2.60 (34.0% ↑)	2.59 (34.2% ↑)

* () : Enhancement ratios.

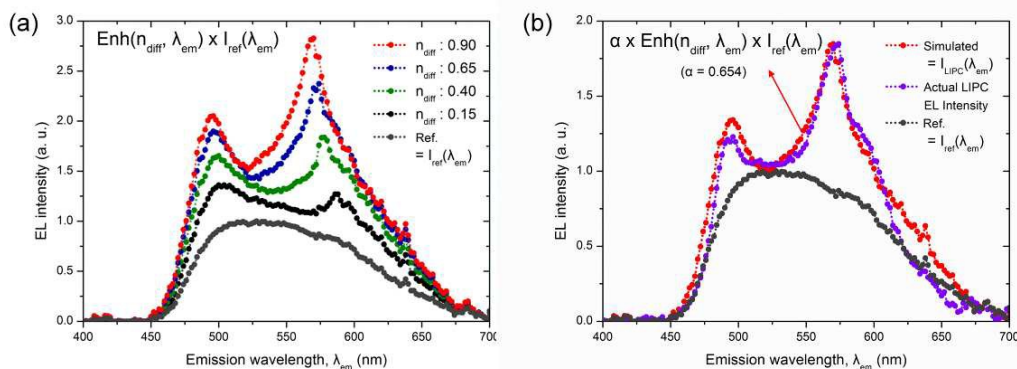


Figure 6. (a) Simulated EL intensity of LIPC-OLED according to n_{diff} applying Equation 4 (before multiplying by the calibration coefficient), and (b) comparison between simulated and actual LIPC-OLED spectra (after multiplying by the calibration coefficient). All data are based on the normalized EL intensity of the reference device, and the actual spectra were obtained at the current density of 20 mA/cm².

It means that the actual EL properties measured in a perpendicular direction may have been slight exaggerated compared to those in an integrating sphere, suggesting that the angular distribution should be clearly analysed in the LIPC-OLED.

Angular distribution

Figure 7(a) shows the simulated results of the angular distributed enhancement factor of LIPC-OLED. In conventional OLEDs, the Lambertian emission is assumed, but for the devices affected by Bragg's diffraction and resonance, the changes in spectrum exist according to the viewing angle. Because the linearity of the light is strengthened in the case of LIPC-OLED, most of the enhancement by the diffraction is found below a viewing angle of 30°. The multi-peak spectra are obvious there, whereas distinct spectral enhancement is not observed when the viewing angle is more than 60°. Even a slight decrease in the efficiency appears in this region; in other words, most of the light encountering the extremely low index layers are changed into a straight direction. As shown in Figure 7(b), this phenomenon appears equally in the measurement of the actual device. As the viewing angle increases, the orange-red peak at 0° is short-wavelength shifted, whereas the blue

peak is extinguished without a spectral change; finally, the peak points are reduced from two to one in the viewing angle of 60°. Also, the enhancement in luminance at same current density (20 mA/cm²) decreases gradually as the viewing angle increases, shown in the inset of Figure 7(b).

Like this, the angular dependence is prominent, but this is a trade-off to obtain a higher efficiency, and the concentrated PC diffraction most of which represented in the low viewing angle caused by enhanced light resonance is clearly positive compared to the conventional PC devices. In addition, we are convinced that these disadvantages will be able to be decreased by extending the LIPC to a higher-dimensional structure (2D rectangular mesh or 2D honeycomb etc.) or by using additional layer like internal planarization layer for lower surface plasmon diffraction or external micro-lens array for the effect of light scattering with reference to previous studies.^{25, 26}

In summary, we investigated the properties of the LIPC-OLED by comparing the actual device information with the simulation. These results mean that the aforementioned two reasons for light extraction were successfully demonstrated, and the design of LIPC-OLED will also be possible by this numerical analysis. Finally, we were able to obtain high-performance and spectrum-predictable OLEDs by inserting a

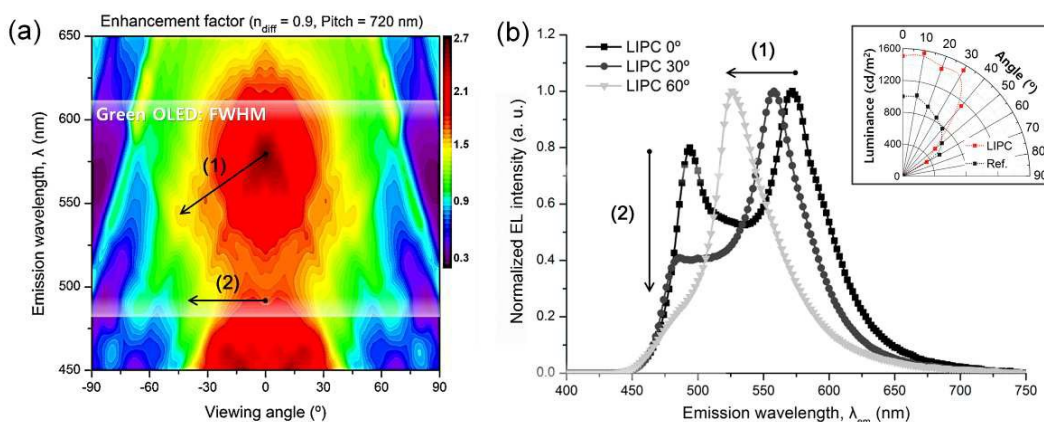


Figure 7. Angular characteristics of LIPC-OLEDs. (a) Simulated angular distribution, (b) Actual device's angular EL intensities and radiative intensity at same current density (20 mA/cm²) depending on the azimuthal angles (the rotation axis and the line-pattern is parallel). The simulated spectral trend lines depending on the changes in viewing angle [(1) and (2)] almost matched the actual device results in the scope of the green FWHM wavelength.

simple nanostructure that can take full advantage of the nano-optics.

Conclusions

We investigated an extremely LIPC layer by utilizing the laser interference lithography process, in which parameters such as period and depth can be easily adjusted through the simple variables of incidence angle and the ratio of solution.

The PC diffraction and the internal light resonance, which are two main causes of enhanced light extraction in LIPC-OLED, can be maximized regarding the larger value of n_{diff} , which is verified by the computational simulation and actual fabrication of the device. Because the increased internal light resonance changes the path of most of the light in straight direction, PC diffraction is more prominent in the low viewing angle, and we were able to obtain high optical efficiency, especially in a forward direction, with the highly extracted TE_0 and TM_0 mode of light in constructive condition. Additionally, the corrugated ITO formed in accordance with the periodic nanopattern and the geometric RI difference of alternately arranged vacuum gap and ITO also contribute to high efficiency by increasing the current density property and the straightness of light in terms of ray tracing.

Although there remain a few points to be improved, this research will be applied in various optical devices as well as in OLEDs that require enhancement at a specific wavelength. Moreover, we expect that these LIPC properties (optional wavelength utilization, strong straightness of light, and high optical efficiency) would be further stabilized in terms of angular distribution when the manufacturing process is extended to a higher-dimensional structure in future research work.

Acknowledgements

This research was supported by the Industry technology R&D program of MOTIE/KEIT (No.10048317), Basic Science Research Program through the National Research Foundation of Korea (NRF) funded by the Ministry of Education, Science and Technology (No. 2012R1A6A3A04039396), the NRF grant funded by the Korea government (MSIP) (CAFDC/Byeong-Kwon Ju/No. 2007-0056090) and IT R&D program of Development of Key Technology for Interactive Smart OLED Lighting, which is a part of ETRI Internal Research Fund.

Notes and references

- M. A. Baldo, D. F. O'Brien, Y. You, A. Shoustikov, S. Sibley, M. E. Thompson, S. R. Forrest, *Nature* 1998, **395**, 151.
- T. Sekitani, H. Nakajima, H. Maeda, T. Fukushima, T. Aida, K. Hata, T. Someya, *Nature Mat.* 2009, **8**, 494.
- T. Kwon, Y. H. Oh, I. Shin, J. I. Hong, *Adv. Funct. Mat.* 2009, **19**, 711.
- S. R. Forrest, D. D. C. Bradley, M. E. Thomson, *Adv. Mater.* 2003, **15**, 1043.
- P. Chou, Y. Chi, *Chem. Eur. J.* 2007, **13**, 380.
- H. Uoyama, K. Goushi, K. Shizu, H. Nomura, C. Adachi, *Nature* 2012, **492**, 234.
- J. W. Huh, J.-W. Shin, D.-H. Cho, J. Moon, C. W. Joo, S. K. Park, J. Hwang, N. S. Cho, J. Lee, J. H. Han, H. Y. Chu, J.-I. Lee, *Nanoscale* 2014, **6**, 10727.
- T. Schwab, C. Fuchs, R. Scholz, A. Zakhidov, K. Leo, M. C. Gather, *Opt. Exp.* 2014, **22**, 7524.
- X.-B. Shi, M. Qian, D.-Y. Zhou, Z.-K. Wang, L.-S. Liao, *J. Mat. Chem. C* 2015, **3**, 1666.
- D. H. Hwang, O. T. Kwon, W. J. Lee, J. W. Hong, T. W. Kim, *Phys. Stat. Sol. A* 2014, **211**, 1773.
- Y. Sun, S. R. Forrest, *Nature* 2008, **2**, 483.
- Y. S. Shim, J. H. Hwang, H. J. Lee, K. B. Choi, K. N. Kim, C. H. Park, S.-G. Jung, Y. W. Park, B. K. Ju, *Adv. Funct. Mat.* 2014, **24**, 6414.
- Y.-J. Lee, S.-H. Kim, J. Huh, G.-H. Kim, Y.-H. Lee, *Appl. Phys. Lett.* 2003, **82**, 3779.
- A. O. Altun, S. Jeon, J. Shim, J.-H. Jeong, D.-G. Choi, K.-D. Kim, J.-H. Choi, S.-W. Lee, E.-S. Lee, H.-D. Park, J. R. Youn, Y.-H. Lee, J.-W. Kang, *Org. Electron.* 2010, **11**, 711.
- M. Fujita, K. Ishihara, T. Ueno, T. Asano, S. Noda, H. Ohata, T. Tsuji, H. Nakada, N. Shimoji, *Jap. J. Appl. Phys.* 2005, **44**, 3669.
- M. Fujita, T. Ueno, K. Ishihara, T. Asano, S. Noda, *Appl. Phys. Lett.* 2004, **85**, 5769.
- Y. Hu, X. Diao, C. Wang, W. Hao, T. Wang, *Vacuum* 2004, **75**, 183.
- S. Jeon, J.-H. Jeong, Y. S. Song, W.-I. Jeong, J.-J. Kim, J. R. Youn, *Nanoscale* 2014, **6**, 2642.
- Y. R. Do, Y.-C. Kim, Y.-H. Lee, *J. Appl. Phys.* 2004, **96**, 7629.
- D.-H. Kim, J. Y. Kim, D.-Y. Kim, J. H. Han, K. C. Choi, *Org. Electron.* 2014, **15**, 3183.
- K. Ishihara, M. Fujita, I. Matsubara, T. Asano, S. Noda, H. Ohata, A. Hirasawa, H. Nakada, N. Shimoji, *Appl. Phys. Lett.* 2007, **90**, 111114.
- W. H. Koo, W. Youn, P. Zhu, X.-H. Li, N. Tansu, F. So, *Adv. Funct. Mat.* 2012, **22**, 3454.
- T. Fuhrmann, K. Samse, J. Salbeck, A. Perschke, H. Franke, *Org. Electron.* 2003, **4**, 219.
- T. W. Koh, J.-M. Choi, S. Yoo, *Adv. Mat.* 2010, **22**, 1849.
- C. Huang, H. Yu, M. Huang, K. Cheng, C. Hsieh, T. Chou, M. Chang, *Appl. Phys. A* 2015, **121**, 449.
- K. B. Choi, S. J. Shin, T. H. Park, H. J. Lee, J. H. Hwang, J. H. Park, B. Y. Hwang, Y. W. Park, B. K. Ju, *Org. Electron.* 2014, **15**, 111.